Electronic Structure of Deformed Carbon Nanotubes

Liu Yang* and Jie Han†
NASA Ames Research Center, MS 230-3, Moffett Field, California 94035
(Received 30 November 1999)

Electronic structure of deformed carbon nanotubes varies widely depending on their chirality and deformation mode. We present a framework to analyze these variations by quantifying the dispersion relation and density of states. The theory is based on the Hückel tight-binding model and confirmed by four orbital tight-binding simulations of nanotubes under stretching, compression, torsion, and bending. It unriddles and unifies previous band gap studies and predicts the shifting, merging, and splitting of Van Hove singularities in the density of state, and the zigzag pattern of band gap change with strains. Possible applications to nanotube devices and spectroscopy research are also presented.

PACS numbers: 71.24.+q, 71.15.Fv, 71.20.Tx, 73.20.Dx

Single wall carbon nanotubes (SWNT) are of great interest in mesoscopic physics and nanotechnology. The predicted 1D electronic structure, especially Van Hove singularities (VHS) [1], has been confirmed and used to interpret experimental spectra obtained from scanning tunneling spectroscopy [2], optical absorption, and resonant Raman scattering [3]. Nanoscale SWNT transistors [4] have been fabricated. In these studies, SWNTs may be subjected to various mechanical deformations, which may correlate to changes in electronic properties. For instance, resistance of SWNT transistors was found to vary significantly under bending and stretching [5]; and an observed torsion of a metallic SWNT was speculated to open a small band gap [6]. Several simulation studies have shown that band gap of semiconducting SWNTs alters widely depending on tube chirality and deformation mode [7–11]. However, these experiments and simulations have yet to be fully understood and bridged by a theory that can provide a concise physics of the electronic coupling to mechanical deformations.

In this Letter, we formulate a framework to predict the dispersion relation and density of states (DOS) of deformed SWNTs using the Hückel tight-binding (TB) model. Significantly, the theory relates shifting of Fermi point $\mathbf{k}_F$ away from Brillouin zone vertices to tube chirality and strain. As a result, the electron states relative to $\mathbf{k}_F$, and hence VHS and band gap, change accordingly to the shift of $\mathbf{k}_F$. This theory unriddles and unifies previous band gap studies and reveals rich band structure. It can be employed to understand and guide experimental studies of nanotube electronic devices and spectra.

Mintmire and White [12] successfully predicted the electronic structure of undeformed SWNTs near Fermi level using the Hückel TB model. We extend their approach to deformed SWNTs. A (n_1, n_2) tube can be viewed as a graphite sheet rolled up into a cylinder along the 2D lattice vector $\mathbf{R} = n_1\mathbf{R}_1 + n_2\mathbf{R}_2$, where $\mathbf{R}_1$ and $\mathbf{R}_2$ are graphene primitive lattice vectors. Electronic states near $\mathbf{k}_F$ can be analyzed from the central Brillouin zone of graphene defined by the reciprocal lattice vectors $\mathbf{K}_i$ satisfying $\mathbf{K}_i \cdot \mathbf{R}_j = 2\pi\delta_{ij}$ in Fig. 1. For an undeformed lattice, the Brillouin zone is hexagonal with $\mathbf{k}_F$ sitting at the vertices $\mathbf{k}_V$. The electronic states of a SWNT allowed by the Born–von Kármán boundary condition $\mathbf{k} \cdot \mathbf{R} = 2\pi m$ lie on parallel lines perpendicular to $\mathbf{R}$. Near $\mathbf{k}_F$ they are characterized by $|\mathbf{k} - \mathbf{k}_F|$. A deformed SWNT by uniaxial and torsional strains can be constructed from a graphite sheet on which a uniform 2D strain tensor $\varepsilon = (\varepsilon_{ij})_{2\times 2}$ is imposed. In the deformed graphene, real space vectors are $\mathbf{r} = (\mathbf{I} + \varepsilon)\mathbf{r}_0$, where $\mathbf{I} = (\delta_{ij})_{2\times 2}$ and subscript 0 denotes undeformed states. We can show [13] that using a $\mathbf{k}$ space transformation $\mathbf{k} = (\mathbf{I} + \varepsilon)^T\mathbf{k}_0$, the Brillouin zone and $\mathbf{k}$ lines remain invariant because in

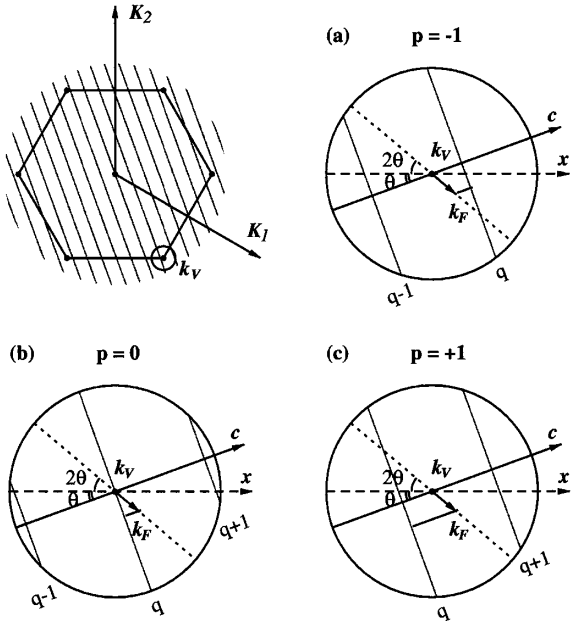

FIG. 1. Top left: hexagonal central Brillouin zone with reciprocal vectors $\mathbf{K}_1$ and $\mathbf{K}_2$, and $\mathbf{k}$ parallel lines for allowed electronic states. Others: pictorial presentation of $\mathbf{k}_F = \mathbf{k}_V + \Delta\mathbf{k}_F$ and Eq. (1) in the circled vertex of the Brillouin zone for three types of SWNTs $n_1 - n_2 = 3q + p$. The $\mathbf{k}_F$ is driven away from the vertex $\mathbf{k}_V$ by uniaxial strain with an angle of 3θ from axis c. The $\mathbf{k}$ lines near $\mathbf{k}_F$ are shown for $m = q$ and $q \pm 1$.

 0031-9007/00/85(1)/154(4)$15.00

the transformed $\mathbf{k}$ space $\mathbf{K}_i \cdot \mathbf{R}_{j0} = \mathbf{K}_{i0} \cdot \mathbf{R}_j = 2\pi\delta_{ij}$ and $\mathbf{k} \cdot \mathbf{R}_0 = \mathbf{k}_0 \cdot \mathbf{R} = 2\pi m$. This approach facilitates analysis of variations in electronic states near $\mathbf{k}_F$ with strains. We need to consider only the change in $\mathbf{k}_F$ relative to invariant $\mathbf{k}$ lines $|\mathbf{k} - \mathbf{k}_F|$.

$\mathbf{k}_F$ is determined by solving $E(\mathbf{k}_F) = |H(\mathbf{k}_F)| = 0$. For deformed graphene, the Hückel TB Hamiltonian is $H(\mathbf{k}) = \Sigma t_j \exp(i\mathbf{k} \cdot \mathbf{r}_{j0})$ with Harrison hopping parameter relation $t_j = t_0(r_0/r_j)^2$ [14]. The sum is over $j = 1, 2, 3$ for three bonds from a carbon atom with a bond length r_j and vector $\mathbf{r}_j = (\mathbf{I} + \varepsilon)\mathbf{r}_{j0}$. Note that the $\mathbf{k}$ space transformation $\mathbf{k} \cdot \mathbf{r}_{j0} = \mathbf{k}_0 \cdot \mathbf{r}_j$ is used in the Hamiltonian. Let $\mathbf{k}_F = \mathbf{k}_V + \Delta\mathbf{k}_F$ with $\mathbf{k}_V = (\mathbf{K}_1 - \mathbf{K}_2)/3$ as circed out in Fig. 1 (equivalent results are obtained for the other inequivalent hexagonal Brillouin zone vertices). By expanding $|H(\mathbf{k}_F)| = 0$ to the first order terms of ε and $\Delta\mathbf{k}_F$, we obtain the following for $\Delta\mathbf{k}_F$ [13]:

$$\begin{aligned} \Delta k_F^c r_0 &= (1 + \nu)\sigma \cos 3\theta + \gamma \sin 3\theta , \\ \Delta k_F^t r_0 &= -(1 + \nu)\sigma \sin 3\theta + \gamma \cos 3\theta . \end{aligned} \tag{1}$$

Superscript t and c denote components along the tube axis and circumference. σ and γ are strains along t and c, corresponding to uniaxial and torsional strains on nanotubes, ν is the Poisson's ratio, and θ is the tube chiral angle.

Equation (1) and $\mathbf{k}_F = \mathbf{k}_V + \Delta\mathbf{k}_F$ are the key to understand and quantify electronic states of deformed SWNTs near Fermi level. They are pictured in Fig. 1 for three types of SWNTs classified by $n_1 - n_2 = 3q + p$ with $p = 0$ (metallic) and ± 1 (semiconducting). From them, we obtain [13] the dispersion relation of deformed graphene by expanding $E(\mathbf{k})$ at $\mathbf{k}_F$,

$$E(\mathbf{k} - \mathbf{k}_F) = \pm|H(\mathbf{k} - \mathbf{k}_F)| = \pm\tfrac{3}{2}t_0 r_0|\mathbf{k} - \mathbf{k}_F| , \tag{2}$$

and then DOS of deformed SWNTs, by following the approach of Ref. [12] and applying the boundary condition $\mathbf{k} \cdot \mathbf{R}_0 = 2\pi m$ to the tube circumference

$$\begin{aligned} \mathrm{DOS}(E) &= \frac{4}{l} \sum_{m=-\infty}^{\infty} \frac{2}{3t_0 r_0}\, g(E, E_m) , \\ g(E, E_m) &= |E|/\sqrt{E^2 - E_m^2} \quad \text{for } |E| > |E_m| , \\ g(E, E_m) &= 0 \quad \text{for } |E| < |E_m| , \\ l &= \left(\frac{1 - \nu\sigma}{1 + \sigma}\right)(\tfrac{2}{3}\sqrt{3})D/r_0^2 , \end{aligned} \tag{3}$$

$$\begin{aligned} |E_m| &= \tfrac{3}{2}t_0 r_0 \Delta k_m^c , \\ \Delta k_m^c &= \left| \frac{2}{3D}[3m - (3q + p)] - \Delta k_F^c \right| , \end{aligned} \tag{4}$$

where l is the central Brillouin zone length, m is the quantum number, and $D = |\mathbf{R}_0|/\pi$ is the tube diameter. Equations (2) and (3) preserve the concise forms of the dispersion relation and DOS of undeformed structures [12]. Strain effects on the VHS intensity and position of DOS are incorporated into l and Δk_F^c through Eqs. (4) and (1), respectively.

The DOS can be calculated using Eqs. (3), (4), and (1). In this work, we take $r_0 = 1.42$ Å, $t_0 = 2.66$ eV, and $\nu = 0.20$. To verify the applicability of the theory which neglects tube curvature effects and higher order terms in expanding $H(\mathbf{k})$, we have carried out simulations of band structure of SWNTs of diverse tube chiralities and diameters under various deformations using a four orbital (s, p_x, p_y, p_z) TB model with parameters from Ref. [15]. The simulation results are consistent with the theoretical predictions. As an example, Fig. 2 plots theoretical and simulation DOS of three SWNTs under stretching deformation. A good agreement between the theory and

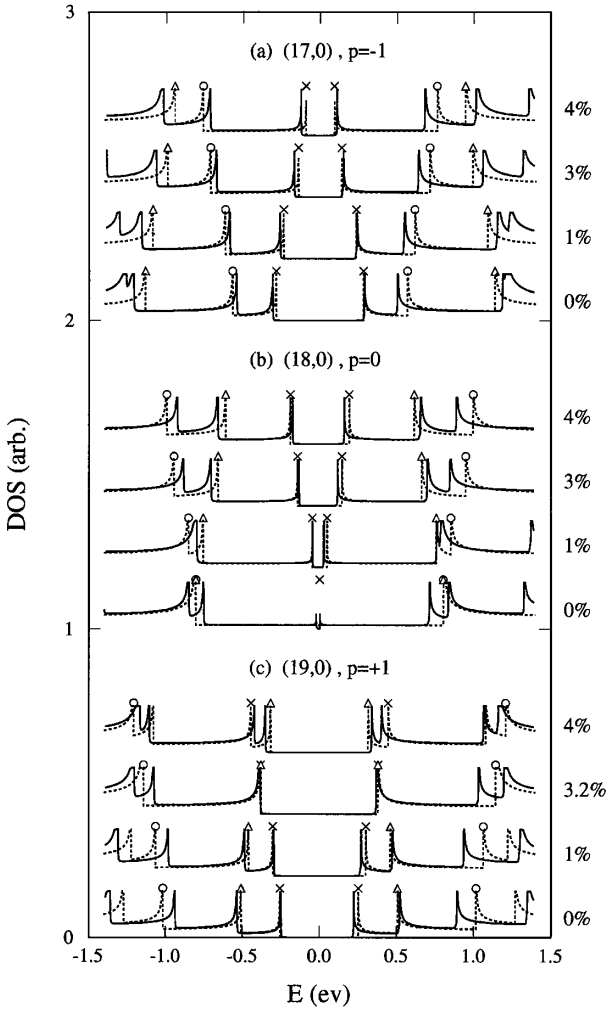

FIG. 2. DOS obtained from theory (solid lines) and simulations (dashed lines) for three types of SWNTs $n_1 - n_2 = 3q + p$ with $q = 6$. Values on the right side are strains. The first, second, and third VHS peaks are labeled by symbols $\times$, $\triangle$, and $\bigcirc$. The critical strains to merge two VHS for tube (19,0) are 2.7% and 3.2% from theory and simulation, respectively. A small band gap of 0.02 eV at zero strain, caused by tube curvature or hybridization effect, is seen by simulation, but not by theory for tube (18,0).

simulations is seen at lower strains and at lower energies. We now use Fig. 1 and Eqs. (4) and (1) to understand the band structure in Fig. 2.

Δk_m^c in Eq. (4) measures the shortest distance between $\mathbf{k}_F$ and $\mathbf{k}$ lines of quantum number m in Fig. 1 and is responsible for the VHS positions E_m in Fig. 2. The smallest E_m equals half the band gap. At zero strains, $\mathbf{k}_F$ sits at $\mathbf{k}_V$. If $\mathbf{k}_V$ is taken as the origin, its nearest allowed $\mathbf{k}$ are at $\frac{2}{3D}$, 0, and $-\frac{2}{3D}$ on the c axis for tubes $p = -1$, 0, and 1, respectively [Eq. (4) with $m = q$ and $\Delta k_F^c = 0$]. For semiconducting tubes $p = \pm 1$, the first nearest distance and VHS at $m = q$ are $\Delta k_q^c = \frac{2}{3D}$ and $|E_q| = t_0 r_0/D$ with a band gap of $2|E_q|$, and the second ones are at $m = q \pm 1$. For metallic tubes $p = 0$, the first nearest distance and band gap are zero at $m = q$, and the second nearest distance is $\mathbf{k}$ line spacing of $\Delta k_{q\pm1}^c = 2/D$, giving rise to the first VHS at $|E_{q\pm1}| = 3t_0 r_0/D$.

When strain drives $\mathbf{k}_F$ to shift away from $\mathbf{k}_V$ by $\Delta\mathbf{k}_F$, VHS positions and band gap change accordingly. The nearest distance Δk_q^c and band gap decrease for $p = -1$ tube but increase for $p = 1$ tube. For metallic tube $p = 0$, a pair of new VHS near $\mathbf{k}_F$ and a band gap [Fig. 2(b) solid lines] are induced. The band gap change under small strains can be derived from Eqs. (1) and (4):

$$\Delta E_{\text{gap}} = \text{sgn}(2p + 1)3t_0[(1 + \nu)\sigma \cos 3\theta + \gamma \sin 3\theta]. \quad (5)$$

Band gap change obtained from Eq. (5) and simulations for various SWNTs under strains up to 1% are presented in Fig. 3. An excellent agreement can be seen. Equation (5) also explains and unifies previous band gap results [7–10]. The previously reported dependence of $\Delta E_{\text{gap}} = 3t_0\sigma$ [7,10] and $3t_0\gamma$ [8,10], respectively, for symmetric zigzag ($\theta = 0$) and armchair ($\theta = \pi/6$) tubes are two special cases of Eq. (5).

We now return to Figs. 1 and 2 for higher strains and other VHS features. As $\mathbf{k}_F$ moves between two $\mathbf{k}$ lines, the first and second nearest distances (Δk_q^c and $\Delta k_{q\pm1}^c$) and VHS positions change in the opposite direction, moving either apart for tubes $p = -1$, or closer for tubes $p = 0$ and 1. The remaining VHS positions vary in alternating directions. We take tube $p = 1$ as an example. The first and second VHS positions get closer as the second and third positions separate. They will merge as $\mathbf{k}_F$ moves to the middle point between two $\mathbf{k}$ lines, i.e., $\Delta k_q^c = \Delta k_{q+1}^c = 1/D$. This leads to a critical strain $\sigma_c = r_0/[3D(1 + \nu)\cos 3\theta]$ and a band gap maximum of $1.5E_{\text{gap},0}$ using Eqs. (4) and (1). Beyond this strain, the merged VHS splits, and the second VHS or Δk_{q+1}^c approaches the Fermi level. This indicates that the band gap maximum at VHS merging is due to electronic states near $\mathbf{k}_F$ jumping from quantum number $m = q$ to $q + 1$. Similar changes and band gap maximum can also be seen for the $p = 0$ tube while a higher critical strain $3\sigma_c$ is required. In contrast, for the $p = -1$ tube, the first pairs of VHS merge as $\mathbf{k}_F$ arrives at the nearest $\mathbf{k}$ line. This results in a semiconductor-metal transition and the required critical strain is $2\sigma_c$. Once the $\mathbf{k}_F$ crosses the $\mathbf{k}$ line, the tube acts as an undeformed metallic tube. For any tubes, as $\mathbf{k}_F$ strolls among the $\mathbf{k}$ lines, it brings periodic shifting, merging, and splitting of two neighboring VHS in DOS, and a zigzag pattern in band gap change. The predicted zigzag pattern and simulation results are illustrated in Fig. 4. The physics and basic features are reproduced although there is a larger discrepancy at higher strains between the theory and simulation. A similar pattern has been observed in previous band gap studies [9] and can be well understood from the present theory.

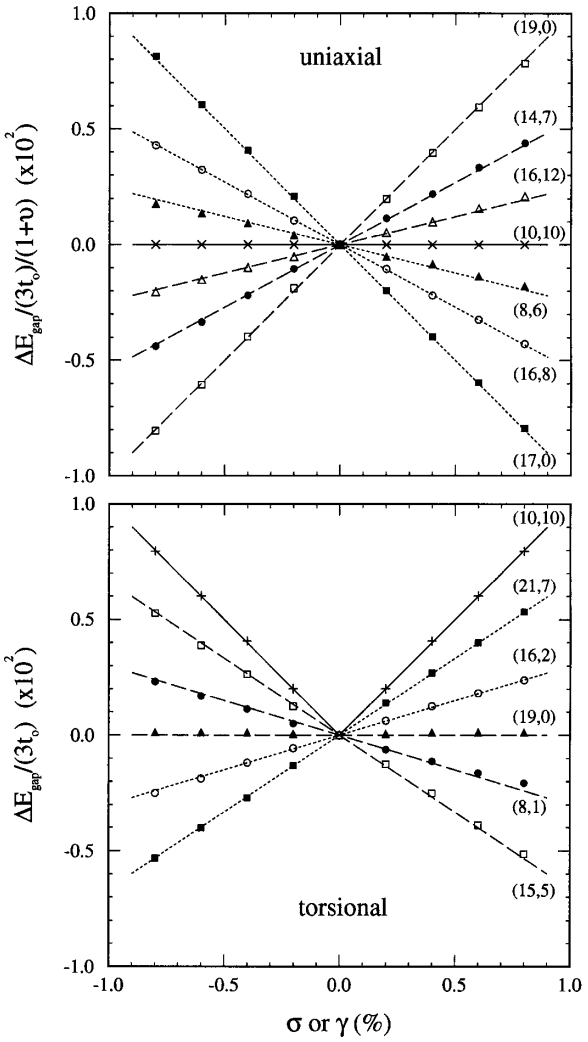

FIG. 3. Band gap change of SWNTs of $\theta = 0 - \pi/6$ and $D = 0.8 - 2.0$ nm, under uniaxial strain (>0 for tension and <0 for compression) and torsional strain (>0 for net bond stretching and <0 for net bond compression), obtained from theory [lines, Eq. (5)] and simulation (symbols).

The above discussion was focused on uniaxial strains. Torsion strain plays similar roles on $\mathbf{k}_F$ and band structure, but the effect of tube chirality is dramatically different for uniaxial and torsion strains by factors $\cos 3\theta$ and $\sin 3\theta$, respectively, as shown in Eq. (1) and Fig. 3. Armchair tubes are inert to uniaxial strain, but sensitive to torsion. Zigzag tubes are the opposite. Other chiral tubes fall in between.

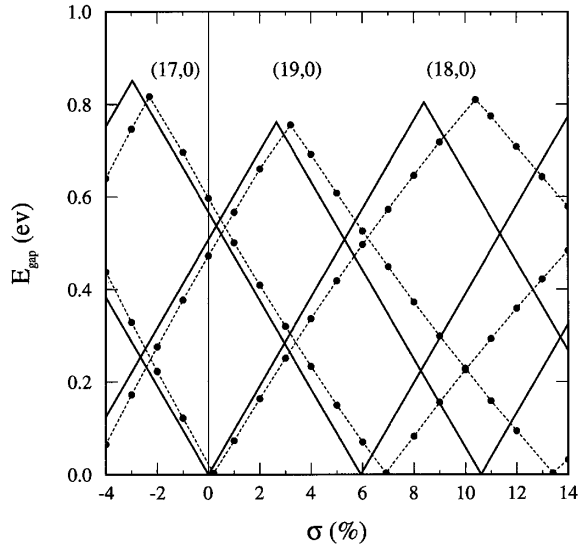

FIG. 4. Zigzag pattern of band gap for three SWNTs under uniaxial strain, obtained from theory (solid lines) and simulations (dashed lines and symbols).

The theory can be extended to tube bending. For pure bending where bond stretching and compression cancel each other along tube circumference, we predict that $\Delta \mathbf{k}_F \cong 0$ for any chiral tube and that VHS position and band gap are invariant while VHS intensity increases on the tensile side and decreases on the compression side [13]. Our four orbital simulations verify this, finding merely a 2% change in VHS position and band gap before the tube buckles. Reference [8] found very weak electronic coupling to bending of armchair tubes, consistent with our results. However, tube bending seen in experiments is usually not pure but accompanied by stretching. Examples are SWNT devices where tube ends are fixed to electrodes or on substrates [3–5]. In these cases, significant change in electronic properties, as observed [5], can be caused by stretching, as well.

The comprehensive DOS results of deformed nanotubes presented in this Letter have many applications to nanotube research. For example, the shift of the $\mathbf{k}_F$ of a nanotube under deformation can change not only electronic properties of the tube itself, but also the contact resistance between the deformed tube and metal electrodes. A low contact resistance can be reached by shifting $\mathbf{k}_F$ of the nanotube to that of the metal electrode [16] through mechanical deformation. Thus, dramatic change in the conductance of deformed nanotubes reported in Ref. [5] may be related to the contact resistance change caused by nanotube $\mathbf{k}_F$ shifting in addition to the tube electronic property change. It has been shown that the width of two VHS peaks is consistent with that of the peaks in the optical adsorption and resonant Raman spectra for SWNT rope samples [3]. Thus, the observed shifting and splitting of the spectral peaks for SWNT ropes may be related to those of VHS peaks caused by deformed nanotubes in the sample. The dependence of VHS peak on tube chirality and deformation presented in this work can be used to analyze the distribution of deformation and tube chirality on individual nanotube as well as tube diameter in the SWNT bundle sample.

In summary, we have formulated the dispersion relation, DOS, and bandgap for deformed SWNTs from the Hückel TB model. The theory preserves the concise form of that of undeformed SWNTs by treating the Fermi point as a function of strains and tube chirality. As the Fermi point is driven by strains to move between and cross over allowed electronic state parallel lines of different quantum numbers, VHS shift, merge, and split, and band gap paves a zigzag pattern. Tube bending effect on DOS and band gap rely on interaction between stretching and compression and can be ignored if stretching and compression cancel each other along the tube circumference. These predicted features have been confirmed by four orbital TB simulations and can be characterized by nanotube electronic device and spectroscopy experiments.

*Electronic address: liuyang@pegasus.arc.nasa.gov
†Electronic address: han@nas.nasa.gov

[1] J. W. Mintmire, B. I. Dunlap, and C. T. White, Phys. Rev. Lett. **68**, 631 (1992); N. Hamada, S. Sawada, and A. Oshiyama, Phys. Rev. Lett. **68**, 1579 (1992); R. Saito, M. Fujita, G. Dresselhaus, and M. S. Dresselhaus, Phys. Rev. B **46**, 1804 (1992).
[2] J. W. G. Wildoer *et al.,* Nature (London) **391**, 59 (1998); T. W. Odom *et al.,* Nature (London) **391**, 62 (1998).
[3] A. M. Rao *et al.,* Science **275**, 187 (1997); H. Kataura *et al.,* Synth. Met. **103**, 2555 (1999); L. Alvarez *et al.,* Chem. Phys. Lett. **316**, 186 (2000).
[4] S. J. Tans, R. M. Vershueren, and C. Dekker, Nature (London) **393**, 49 (1998); R. Martel *et al.,* Appl. Phys. Lett. **73**, 2447 (1998).
[5] W. Thomas *et al.,* Appl. Phys. Lett. **76**, 2414 (2000).
[6] W. Clauss, D. J. Bergeron, and A. T. Johnson, Phys. Rev. B **58**, R4266 (1998).
[7] R. Hyed, A. Charlier, and E. McRae, Phys. Rev. B **55**, 6820 (1997).
[8] C. L. Kane and E. J. Mele, Phys. Rev. Lett. **78**, 1932 (1997).
[9] D. W. Brenner *et al.,* J. Br. Interplanet. Soc. **51**, 137 (1998).
[10] L. Yang, M. P. Anantram, J. Han, and J. P. Lu, Phys. Rev. B **60**, 13 874 (1999).
[11] A. Rocherfort, D. R. Salahub, and Ph. Avouris, Chem. Phys. Lett. **297**, 45 (1998).
[12] J. W. Mintmire and C. T. White, Phys. Rev. Lett. **81**, 2506 (1998); C. T. White and J. W. Mintmire, Nature (London) **394**, 29 (1998).
[13] Liu Yang and Jie Han (unpublished).
[14] W. A. Harrison, *Electronic Structure and the Properties of Solids: The Physics of the Chemical Bond* (Freeman, San Francisco, 1990).
[15] D. Tomanek and S. G. Louie, Phys. Rev. B **37**, 8327 (1988).
[16] J. Tersoff, Appl. Phys. Lett. **74**, 2122 (1999); P. Delaney and M. D. Ventra, Appl. Phys. Lett. **75**, 4028 (1999).